COMMUN. MATH. SCI.
Vol. 11, No. 1, pp. 315–343

PATTERN FORMATION IN RAYLEIGH–BÉNARD CONVECTION*

TAYLAN SENGUL† AND SHOUHONG WANG‡

Abstract. The main objective of this article is to study the three-dimensional Rayleigh-Bénard convection in a rectangular domain from a pattern formation perspective. It is well known that as the Rayleigh number crosses a critical threshold, the system undergoes a Type-I transition, characterized by an attractor bifurcation. The bifurcated attractor is an $(m-1)$–dimensional homological sphere, where m is the multiplicity of the first critical eigenvalue. When $m=1$, the structure of this attractor is trivial. When $m=2$, it is known that the bifurcated attractor consists of steady states and their connecting heteroclinic orbits. The main focus of this article is then on the pattern selection mechanism and stability of rolls, rectangles, and mixed modes (including hexagons) for the case where $m=2$. We derive in particular a complete classification of all transition scenarios, determining the patterns of the bifurcated steady states, their stabilities, and the basin of attraction of the stable ones. The theoretical results lead to interesting physical conclusions, which are in agreement with known experimental results. For example, it is shown in this article that only the pure modes are stable whereas the mixed modes are unstable.

Key words. Rayleigh-Bénard convection, pattern formation, rolls, rectangles, hexagons, dynamic transitions.

AMS subject classifications. 35Q, 76, 86.

1. Introduction

Over the years, the Rayleigh-Bénard convection problem, together with the Taylor problem, has become one of the paradigms for studying nonequilibrium phase transitions and pattern formation in nonlinear sciences. There is an extensive literature on the subject; see e.g. reviews by Busse [1], Chandrasekhar [2], Cross & Hohenberg [3], Getling [5], Koschmieder [6], Lappa [7], Ma & Wang [8], and the references therein.

The problem is complete from the dynamic transition perspective (Ma and Wang [9, 10]). The main result in this direction is that the system always undergoes a Type-I (continuous) transition as the instability driving mechanism, the Rayleigh number, crosses a critical threshold R_c, thanks to the symmetry of the linear operator, properties of the nonlinearity, and the asymptotic stability of the basic state at the critical threshold. Moreover, the system has a bifurcated attractor which is an $(m-1)$–dimensional homological sphere, where m is the number of critical eigenvalues of the linear operator.

The main objective of this paper is to study pattern formation and the structure of the bifurcated attractor for the Rayleigh–Bénard convection. The structure of the bifurcated attractor is trivial when $m=1$. Namely, the attractor consists of two attracting steady states approximated by the critical mode with opposite flow orientations.

When $m \geq 2$, the picture is far from being complete. There are some known characteristics of this attractor such as the attractor must be homeomorphic to S^1,

*Received: September 26, 2011; accepted (in revised form): May 21, 2012. Communicated by Andrea Bertozzi.
The work was supported in part by the Office of Naval Research and by the National Science Foundation.

†Department of Mathematics, Indiana University, Bloomington, IN 47405, USA (msengul@indiana. edu).

‡Department of Mathematics, Indiana University, Bloomington, IN 47405, USA (showang@indiana. edu, http://www.indiana.edu/~fluid).

and either contains four or eight steady states connected by heteroclinic orbits or is a circle of steady states.

In general the relation between the two horizontal length scales for a given multiplicity $m \geq 2$ is nonlinear, as shown in figure 4.1. One of the main objectives of this article is to present a general approach for studying transitions for $m \geq 2$. For simplicity, we consider only the case where the wave numbers of the critical modes are equal. Under this assumption we are able to give a complete characterization for the case $m = 2$; the general case $m \geq 2$ can be studied in a similar fashion.

Also, we remark that, for a given $m \geq 2$, the set of all (L_1, L_2) in the L_1-L_2 plane is of measure zero; see figure 4.1. However, from a pattern formation point of view, most interesting patterns appear in these non-generic cases. Meanwhile, when the length scales are close to those length scales for which $m = 2$, a critical mode at the critical Rayleigh number R_c appears first, followed closely by a second critical mode near R_c. This will lead to the similar transition scenarios as described in this article.

Depending on its horizontal wave indices i_x and i_y, a single critical mode can be either a roll (when at least one of i_x or i_y is zero) or a rectangle (when both i_x and i_y are non-zero), where i_x and i_y are non-negative integers which cannot vanish together. Thus there are three possible cases: (a) one of the critical modes is a roll while the other one is a rectangle, (b) both critical modes are rolls, (c) both critical modes are rectangles.

In each case, we explicitly find nondimensional numbers which determine the number, patterns, and stabilities of the bifurcated steady states. We also determine the basin of attraction of each of the stable steady states.

In all the scenarios, we found that after the transition, only pure modes (rolls or rectangles) are stable and the mixed modes are unstable. Our result is conclusive when one of the critical modes is a roll type. When both critical modes are rectangles, we only have computational evidence.

When both critical modes are rolls, the stable steady states after the transition are rolls. When both critical modes are rectangles, computational evidence suggests that the stable steady states after the transition are rectangles. When one critical mode is a roll and the other one is a rectangle, the stable states after the transition can be either only rolls or both rolls and rectangles.

The problem is usually studied in the infinitely extended horizontal domain setting, which eliminates the effects of the boundaries in the horizontal directions. Our setting is a 3D rectangular domain with free-slip boundary conditions for the velocity, that is, the fluid can not cross the boundaries but is allowed to slip. The thermal boundary conditions are adiabatically isolated side walls, so that no heat is transferred through them, and perfectly conducting top and bottom boundaries.

Technically, the analysis is carried out using the dynamical transition theory (Ma and Wang [8]). One key ingredient is the reduction of the original system to the center manifold generated by the two unstable modes. The only modification that has been made is, following Sengul and Wang [13], we expand the center manifold using a basis which differs from the eigenfunctions of the original linear operator. This allows us to circumvent the difficulties associated with determining the eigenpairs in terms of the system parameters. We also make use of computer assistance, namely Mathematica, which carries out numerous integrations which are due to the interactions of the critical modes with the non-critical ones.

The paper is organized as follows: In Section 2, the governing equations and the functional setting of the problem are introduced. Section 3 deals with the linear

theory. We present our main results in Section 4. The proof of these theorems are given in Section 5. In Section 6, we present the physical conclusions derived from our theorems. Finally, Section 7 is the conclusion section.

2. Governing equations and the functional setting

With the Boussinesq approximation, the non-dimensional equations governing the motion and the states of the Rayleigh-Bénard convection in a nondimensional rectangular domain $\Omega=(0,L_1)\times(0,L_2)\times(0,1)\subset\mathbb{R}^3$ are given as follows (see [2] among others):

$$\begin{aligned}
&\frac{\partial \mathbf{u}}{\partial t}+(\mathbf{u}\cdot\nabla)\mathbf{u}=\Pr(-\nabla p+\Delta\mathbf{u}+R\theta\mathbf{k}),\\
&\frac{\partial \theta}{\partial t}+(\mathbf{u}\cdot\nabla)\theta=w+\Delta\theta,\\
&\nabla\cdot\mathbf{u}=0,\\
&\mathbf{u}(0)=\mathbf{u}_0,\quad \theta(0)=\theta_0.
\end{aligned}\tag{2.1}$$

The unknown functions are the velocity $\mathbf{u}=(u,v,w)$, the temperature θ, and the pressure p. These unknowns represent a deviation from a motionless state basic steady state with a constant positive vertical temperature gradient. In addition, $\mathbf{k}$ stands for the unit vector in the z-direction.

The non-dimensional numbers in (2.1) are the Rayleigh number R, which is the control parameter, and Pr, the Prandtl number.

The above system is supplemented with a set of boundary conditions. We use the free-slip boundary conditions for the velocity on all the boundaries. Thermally, the top and the bottom boundaries are assumed to be perfectly conducting and the horizontal boundaries are adiabatically isolated. Namely, the boundary conditions are as follows:

$$\begin{aligned}
&u=\frac{\partial v}{\partial x}=\frac{\partial w}{\partial x}=\frac{\partial \theta}{\partial x}=0 \quad \text{at } x=0,L_1,\\
&\frac{\partial u}{\partial y}=v=\frac{\partial w}{\partial y}=\frac{\partial \theta}{\partial y}=0 \quad \text{at } y=0,L_2,\\
&\frac{\partial u}{\partial z}=\frac{\partial v}{\partial z}=w=\theta=0 \qquad \text{at } z=0,1.
\end{aligned}\tag{2.2}$$

For the functional setting, we define the relevant function spaces:

$$\begin{aligned}
&H=\left\{(\mathbf{u},\theta)\in L^2\left(\Omega,\mathbb{R}^4\right):\nabla\cdot\mathbf{u}=0,\mathbf{u}\cdot n\,|_{\partial\Omega}=0\right\},\\
&H_1=\left\{(\mathbf{u},\theta)\in H^2\left(\Omega,\mathbb{R}^4\right):\nabla\cdot\mathbf{u}=0,\mathbf{u}\cdot n\,|_{\partial\Omega}=0,\theta\,|_{z=0,1}=0\right\}.
\end{aligned}\tag{2.3}$$

For $\phi=(\mathbf{u},\theta)$, let $G:H_1\to H$ and $L_R:H_1\to H$ be defined by

$$\begin{aligned}
&L_R\phi=(\Pr\mathcal{P}(\Delta\mathbf{u}+R\theta\mathbf{k}),w+\Delta\theta),\\
&G(\phi)=-(\mathcal{P}(\mathbf{u}\cdot\nabla)\mathbf{u},(\mathbf{u}\cdot\nabla)\theta),
\end{aligned}\tag{2.4}$$

with $\mathcal{P}$ denoting the Leray projection onto the divergence-free vectors. The equations (2.1) and (2.2) can be put into the following functional form:

$$\frac{d\phi}{dt}=L_R\phi+G(\phi),\qquad \phi(0)=\phi_0.\tag{2.5}$$

The results concerning existence and uniqueness of (2.5) are classical and we refer the interested readers to Foias, Manley, and Temam [4] for details. In particular, we can define a semigroup

$$S(t):\phi_0\to\phi(t).$$

Finally for $\phi_i=(\mathbf{u}_i,\theta_i)$, $i=1,2,3$ we define the following trilinear forms, which will be used in the proof of the main theorems:

$$\begin{aligned} G(\phi_1,\phi_2,\phi_3)&=-\int_\Omega(\mathbf{u_1}\cdot\nabla)\mathbf{u_2}\cdot\mathbf{u_3}-\int_\Omega(\mathbf{u_1}\cdot\nabla)\theta_2\cdot\theta_3,\\ G_s(\phi_1,\phi_2,\phi_3)&=G(\phi_1,\phi_2,\phi_3)+G(\phi_2,\phi_1,\phi_3). \end{aligned} \tag{2.6}$$

3. Linear theory

We recall in this section the well-known linear theory of the problem.

3.1. Linear eigenvalue problem. We first study the eigenvalue problem

$$\begin{aligned} &\mathrm{Pr}(\Delta\mathbf{u}+R\theta\mathbf{k}-\nabla p)=\beta\mathbf{u},\\ &w+\Delta\theta=\beta\theta,\\ &\mathrm{div}\mathbf{u}=0, \end{aligned} \tag{3.1}$$

with the boundary conditions (2.2). Thanks to the boundary conditions, we can represent the solutions $\phi_S=(\mathbf{u}_S,\theta_S)$, $\mathbf{u}_S=(u_S,v_S,w_S)$ by the separation of variables

$$\begin{aligned} u_S&=U_S\sin(L_1^{-1}s_x\pi x)\cos(L_2^{-1}s_y\pi y)\cos(s_z\pi z),\\ v_S&=V_S\cos(L_1^{-1}s_x\pi x)\sin(L_2^{-1}s_y\pi y)\cos(s_z\pi z),\\ w_S&=W_S\cos(L_1^{-1}s_x\pi x)\cos(L_2^{-1}s_y\pi y)\sin(s_z\pi z),\\ \theta_S&=\Theta_S\cos(L_1^{-1}s_x\pi x)\cos(L_2^{-1}s_y\pi y)\sin(s_z\pi z), \end{aligned} \tag{3.2}$$

for $S=(s_x,s_y,s_z)$, where $s_x\geq0$, $s_y\geq0$, $s_z\geq0$. It is easy to see that only eigenvalues β_S, $S\in\mathcal{Z}$ can become positive, where

$$\mathcal{Z}=\{(s_x,s_y,s_z)\,|\,s_x\geq0,\ s_y\geq0,\ s_z\geq0,\ (s_x,s_y)\neq(0,0)\text{ and }s_z\neq0\}.$$

For $S=(s_x,s_y,s_z)\in\mathcal{Z}$, the amplitudes of the horizontal velocity field can be found as

$$U_S=-\frac{s_x\pi}{L_1}\frac{s_z\pi}{\alpha_S^2}W_S,\qquad V_S=-\frac{s_y\pi}{L_2}\frac{s_z\pi}{\alpha_S^2}W_S.$$

We define α_S, the horizontal wave number and γ_S, the full wave number by

$$\alpha_S=\sqrt{\frac{s_x^2\pi^2}{L_1^2}+\frac{s_y^2\pi^2}{L_2^2}},\qquad \gamma_S=\sqrt{\frac{s_x^2\pi^2}{L_1^2}+\frac{s_y^2\pi^2}{L_2^2}+s_z^2\pi^2}. \tag{3.3}$$

Taking the divergence of the first equation in (3.1), we find

$$\Delta p=R\frac{\partial\theta}{\partial z}.$$

Now, taking the Laplacian of the first equation, replacing Δp by the above relation, and using (3.2), we obtain

$$\begin{aligned} &\gamma_S^2(\mathrm{Pr}\,\gamma_S^2+\beta)W_S-R\,\mathrm{Pr}\,\alpha_S^2\Theta_S=0,\\ &W_S-(\gamma_S^2+\beta)\Theta_S=0. \end{aligned} \tag{3.4}$$

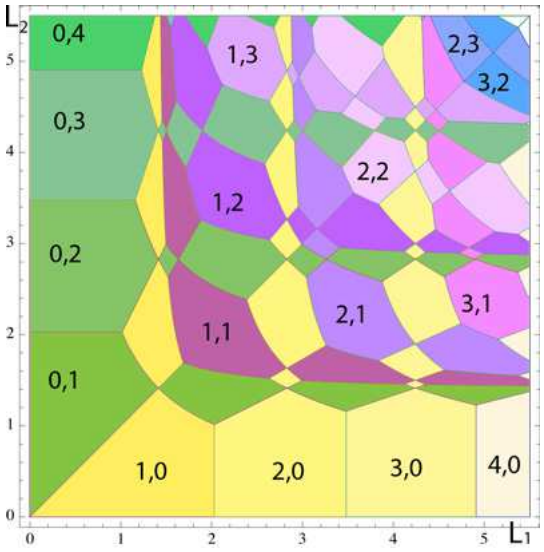

FIG. 3.1. *The selection of critical horizontal wave indices in the L_1–L_2 plane. The same coloring indicates equal wave indices.*

For each $S \in \mathcal{Z}$, the above equations have two solutions $\beta_S^1 > \beta_S^2$, which satisfy the following equation:

$$\gamma_S^2(\gamma_S^2+\beta)(\mathrm{Pr}\,\gamma_S^2+\beta) - R\,\mathrm{Pr}\,\alpha_S^2 = 0. \tag{3.5}$$

We find the amplitudes of the normalized critical eigenvectors as

$$W_S = \beta_S^1(R) + \gamma_S^2, \qquad \Theta_S = 1. \tag{3.6}$$

Now solving (3.5) for R at $\beta = 0$, the critical Rayleigh number can be defined as

$$R_c = \min_{S\in\mathcal{Z}} R_S, \qquad R_S := \frac{\gamma_S^6}{\alpha_S^2}. \tag{3.7}$$

From (3.7), one sees that for a minimizer $S = (s_x, s_y, s_z)$ of R_S, the vertical index s_z is 1. We will denote the set of critical indices S minimizing (3.7) by $\mathcal{C}$:

$$\mathcal{C} = \{S = (s_x, s_y, 1) \in \mathcal{Z} \mid R_S \le R_{S'}, \forall S' \in \mathcal{Z}\}.$$

For small length scale region, the map in figure 3.1 shows the horizontal critical wave indices that are picked by the selection mechanism (3.7).

It is well known that we have the following PES condition:

$$\beta_S^1(R) \begin{cases} <0, & \lambda < R_c, \\ =0, & \lambda = R_c, \\ >0, & \lambda > R_c, \end{cases} \qquad \forall S \in \mathcal{C}, \tag{3.8}$$

$$\Re\beta(R_c) < 0, \qquad \forall \beta \notin \{\beta_S^1 \mid S \in \mathcal{C}\}. \tag{3.9}$$

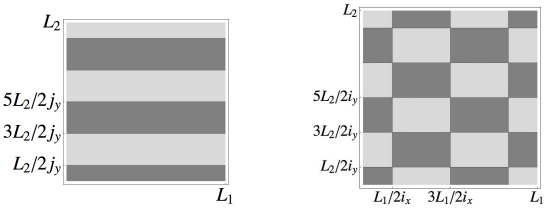

(a) A roll pattern with wave index $J=(0,j_y,1)$.

(b) A rectangle pattern with wave index $I=(i_x,i_y,1)$.

FIG. 3.2. *Regions of positive and negative vertical velocity of a rectangular and a roll mode at the mid-plane* $z=1/2$.

By (3.5), corresponding to $S=(s_x,s_y,s_z)\in\mathcal{Z}$, there are two eigenvalues β_S^i and two corresponding eigenfunctions ϕ_S^i, $i=1,2$. If a critical mode has wave index I then the corresponding eigenfunction is ϕ_I^1, which we will simply denote by ϕ_I.

Depending on the horizontal wave indices, there are two types of critical modes corresponding to two different patterns. If the wave index $I=(i_x,i_y,1)$ of a critical mode is such that one of the horizontal wave indices i_x, i_y is zero, the corresponding eigenfunction has a roll pattern. When both horizontal indices are non-zero, the corresponding eigenfunction has a rectangular pattern. Figure 3.2 shows a sketch of these patterns.

3.2. Estimation of the critical wave number. As it will be shown, the dynamic transitions depend on the critical wavenumber α. In the case of infinite horizontal domains, the critical wave number is found to be $\alpha=\pi/\sqrt{2}\approx 2.22$, corresponding to a critical Rayleigh number $R_c=27\pi^4/4\approx 658$. For rectangular domains, the wave number is not constant and is a function of the length scales. The following estimates will be important in the physical remarks section.

LEMMA 3.1. *Let* α *be the critical wave number minimizing* (3.7). *Then*

$$\alpha\geq\frac{\pi}{2^{1/3}(2^{2/3}+1)^{1/2}}\approx 1.55,\quad \textit{for all } L_1,L_2,$$
$$\alpha<\frac{2^{2/3}\pi}{\sqrt{1+2^{2/3}}}\approx 3.10,\quad \textit{if } L_1>2^{1/3}\sqrt{1+2^{2/3}}\approx 2.03,$$
$$\alpha\to\frac{\pi}{\sqrt{2}},\quad L_1\to\infty.$$

Proof. To estimate the dependence of the wave number α on the length scales L_1, L_2, we define

$$L(m)=((m+1)m)^{1/3}((m+1)^{2/3}+m^{2/3})^{1/2},\quad m\in\mathbb{Z},\ m\geq 0.$$

The sequence $L(m)$ gives those length scales of L_1 for which the wave index changes, assuming L_2 is sufficiently small. As shown in Sengul and Wang [13], when $L(m-1)<L_1<L(m)$ for some $m\geq 1$, we have the following bound on the critical wave number:

$$\frac{m\pi}{L(m)}<\alpha<\frac{m\pi}{L(m-1)}. \tag{3.10}$$

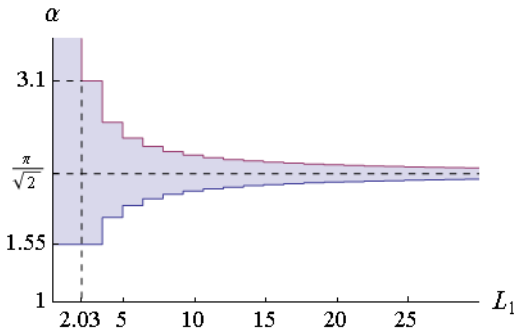

FIG. 3.3. *The shaded region shows the possible values for the critical wave number α for a given L_1.*

In particular,

$$\alpha \geq \frac{\pi}{L(1)} = \frac{\pi}{2^{1/3}(2^{2/3}+1)^{1/2}}$$

and

$$\alpha \leq \frac{2\pi}{L(1)} = \frac{2^{2/3}\pi}{\sqrt{1+2^{2/3}}}, \quad \text{if } L_1 > L(1).$$

Finally noticing that,

$$\frac{m\pi}{L(m)} \to \frac{\pi}{\sqrt{2}}, \quad \frac{(m+1)\pi}{L(m)} \to \frac{\pi}{\sqrt{2}}, \quad \text{as } m \to \infty,$$

we find that

$$\alpha \to \frac{\pi}{\sqrt{2}}, \quad L_1 \to \infty.$$

□

The bounds on the critical wave number as a function of the length scale L_1 which is obtained from (3.10) is shown in figure 3.3.

4. Dynamic transitions and pattern selection

We study the case where two eigenvalues with indices $I=(i_x,i_y,1)$ and $J=(j_x,j_y,1)$ are the first critical eigenvalues. This means that α_I and α_J minimize (3.7), thus the PES conditions (3.8), (3.9) are satisfied with $\mathcal{C}=\{I,J\}$. The crucial assumption is that the corresponding wave numbers are equal, i.e.

$$\alpha = \alpha_I = \alpha_J.$$

Since $I \neq J$, without loss of generality we can assume that $i_x > j_x$ which ensures that $i_y < j_y$. By (3.3), we must have the following linear relation between the length scales:

$$L_1 = \sqrt{\frac{i_x^2 - j_x^2}{j_y^2 - i_y^2}} L_2.$$

Thus two critical eigenmodes are possible only when L_1 and L_2 lie on a line emanating from the origin in figure 4.1. There are three possible cases depending on the structure of the critical eigenmodes, which are completely described by our main theorems:

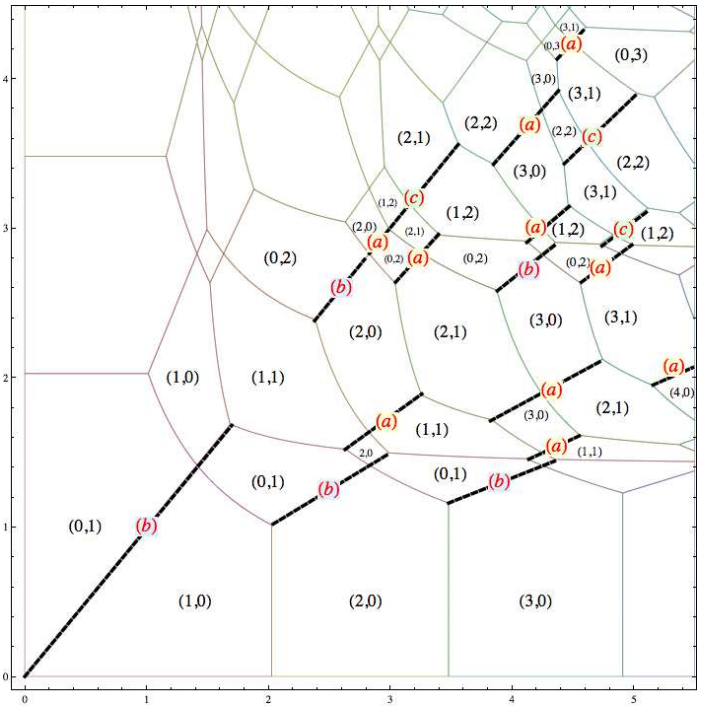

FIG. 4.1. *The first two critical modes with (a) a rectangle and a roll pattern, (b) both roll patterns, (c) both rectangle patterns.*

(a) a rectangle and a roll mode respectively (described by Theorem 4.1),

(b) both roll modes (described by Theorem 4.2),

(c) both rectangle modes (described by Theorem 4.3).

These possible cases are illustrated by figure 4.1 in the small length scale regime.

Before presenting our results, we first summarize some of the known results which apply in the above setting (see Ma and Wang [9, 10]):

i) As the Rayleigh number R crosses R_c, the system undergoes a Type-I (continuous) transition.

ii) There is an attractor Σ_R bifurcated on $R > R_c$ such that for any $\phi_0 \in H \setminus \Gamma$,

$$dist(\phi_0, \Sigma_R) \to 0, \quad \text{as } t \to \infty,$$

where Γ is the stable manifold of $\phi = 0$ with $codim = 2$.

iii) Σ_R is homeomorphic to S^1 and comprises steady states and the heteroclinic orbits connecting these steady states.

iv) There are four or eight bifurcated steady states. Half of the bifurcated steady states are minimal attractors and the rest are saddle points.

The dynamic transitions depend on the following *positive* parameter which in

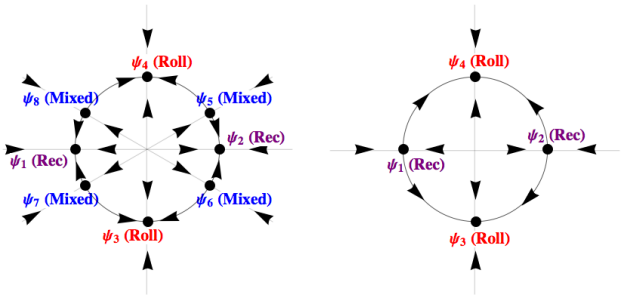

(a) When $a<c$. (b) When $c<a$.

FIG. 4.2. *The structure of the attractor after the transition $R>R_c$ for different parameter regions when the first two critical modes are a roll and a rectangle.*

turn is a function of the parameters Pr, L_1, and L_2:

$$\kappa_S = \begin{cases} \frac{1}{16}\frac{\mathrm{Pr}}{1+\mathrm{Pr}}\gamma^4, & S=(0,0,2), \\ \frac{\pi^2(4\alpha^2-\alpha_S^2)^2}{(R_S-R_c)\alpha^6}\frac{R_c}{2^7(1+\mathrm{Pr})}\left(\mathrm{Pr}^{-1}\gamma_S^2\gamma^2+2\gamma^4+\mathrm{Pr}\,R_S\alpha^2\gamma_S^{-2}\right), & S\neq(0,0,2). \end{cases} \tag{4.1}$$

Here, α is the critical wave number, $\gamma^2=\alpha^2+\pi^2$, and $R_c=\gamma^6/\alpha^2$ is the critical Rayleigh number. Moreover, for $S=(s_x,s_y,s_z)$, $(s_x,s_y)\neq(0,0)$:

$$\alpha_S^2=\frac{s_x^2\pi^2}{L_1^2}+\frac{s_y^2\pi^2}{L_2^2}, \quad \gamma_S^2=\alpha_S^2+s_z^2\pi^2, \quad R_S=\frac{\gamma_S^6}{\alpha_S^2}.$$

Also we let

$$g=\frac{\mathrm{Pr}\,\alpha^2}{(\mathrm{Pr}+1)\gamma^4}.$$

4.1. One of the critical modes is a roll, the other is a rectangle. We first consider the case where an eigenmode with a roll structure and an eigenmode with a rectangle structure are the first critical eigenmodes.

THEOREM 4.1. *Assume that $I=(i_x,i_y,1)$ and $J=(0,j_y,1)$ ($i_x\geq 1$, $j_y>i_y\geq 1$) are the first critical indices with identical wave numbers, $\alpha_I=\alpha_J$.* Consider the following numbers:

$$\begin{aligned} a&=\kappa_{0,0,2}+\kappa_{2i_x,0,2}+\kappa_{0,2i_y,2}, \\ b&=\kappa_{0,0,2}, \\ c&=\kappa_{0,0,2}+2\kappa_{i_x,i_y+j_y,2}+2\kappa_{i_x,-i_y+j_y,2}. \end{aligned} \tag{4.2}$$

For $R>R_c$, let us define the following steady state solutions:

$$\psi_i=g\sqrt{R-R_c}(X_i\phi_I+Y_i\phi_J)+o((R-R_c)^{1/2}), \quad i=1,\ldots,8,$$

where

$$\begin{aligned} &X_i=(-1)^i a^{-1/2}, \quad Y_i=0, && i=1,2, && \text{(rectangle pattern)} \\ &X_i=0, && Y_i=(-1)^i(2b)^{-1/2}, && i=3,4, && \text{(roll pattern)} \end{aligned}$$

$$X_i = \sqrt{\frac{c-b}{c^2-ab}}, \qquad Y_i = (-1)^i \sqrt{\frac{c-a}{2(c^2-ab)}}, \qquad i=5,6, \qquad \text{(mixed pattern)}$$

$$X_i = -\sqrt{\frac{c-b}{c^2-ab}}, \qquad Y_i = (-1)^i \sqrt{\frac{c-a}{2(c^2-ab)}}, \qquad i=7,8. \qquad \text{(mixed pattern)}$$

There are two possible transition scenarios:

i) If $a<c$ then the topological structure of the system after the transition is as in figure 4.2(a). In particular,
   1) Σ_R contains eight steady states ψ_i, $i=1,\dots,8$.
   2) ψ_1, ψ_2 (rectangles) and ψ_3, ψ_4 (rolls) are minimal attractors of Σ_R, whereas ψ_5, ψ_6, ψ_7, and ψ_8 (mixed) are unstable.
   3) There is a neighborhood $\mathcal{U}\setminus\Gamma$ of 0, where Γ is the stable manifold of 0, such that $\bar{\mathcal{U}} = \cup_{i=1}^4 \bar{\mathcal{U}}_i$, with $\mathcal{U}_i$ pairwise disjoint, and where $\mathcal{U}_i$ is the basin of attraction of ψ_i, $i=1,\dots,4$.
   4) The projection of $\mathcal{U}_i$ onto the space spanned by ϕ_I, ϕ_J is approximately a sectorial region given by

$$\mathcal{U}_i \cap \{X\phi_I + Y\phi_J \,|\, \omega_{i,1} < arg(X,Y) < \omega_{i,2}\}, \quad i=1,\dots,4,$$

$$\omega_{1,1}=\pi-\omega, \quad \omega_{1,2}=\pi+\omega, \quad \omega_{2,1}=-\omega, \quad \omega_{2,2}=\omega,$$
$$\omega_{3,1}=\pi+\omega, \quad \omega_{3,2}=2\pi-\omega, \quad \omega_{4,1}=\omega, \quad \omega_{4,2}=\pi-\omega,$$

   where

$$\omega = \arctan\sqrt{\frac{c-a}{2(c-b)}}. \tag{4.3}$$

ii) If $c<a$ then the topological structure of the system after the transition is as in figure 4.2(b). In particular,
   a) Σ_R contains four steady states ψ_i, $i=1,\dots,4$.
   b) ψ_3, ψ_4 (rolls) are minimal attractors of Σ_R, whereas the ψ_1, ψ_2 (rectangles) are unstable steady states.
   c) There is a neighborhood $\mathcal{U}\setminus\Gamma$ of 0, where Γ is the stable manifold of 0, such that $\bar{\mathcal{U}} = \cup_{i=3}^4 \bar{\mathcal{U}}_i$, with $\mathcal{U}_i$ pairwise disjoint, and where $\mathcal{U}_i$ is the basin of attraction of ψ_i, $i=3,4$.
   d) The projection of $\mathcal{U}_i$ onto the space spanned by ϕ_I, ϕ_J is a sectorial region given by

$$\mathcal{U}_i \cap \{X\phi_I + Y\phi_J \,|\, \omega_{i,1} < arg(X,Y) < \omega_{i,2}\}, \quad i=3,4,$$

$$\omega_{3,1}=\pi, \ \omega_{3,2}=2\pi, \quad \omega_{4,1}=0, \ \omega_{4,2}=\pi.$$

REMARK 4.1. In the special case $j_y = 2i_y$, the mixed solution corresponds to a regular hexagonal pattern. In this case we find $a<c$, hence the first scenario in Theorem 4.1 is valid; see Remark 5.1.

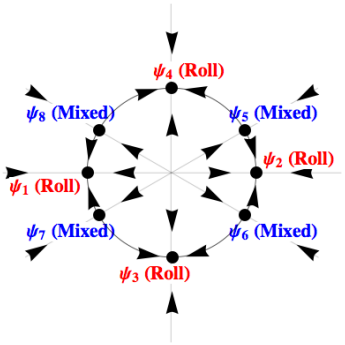

FIG. 4.3. *The structure of the attractor after the transition $R > R_c$, when the first two critical modes are both roll type.*

4.2. The first two critical modes are both rolls. In this section we consider two critical modes both having a roll structure. Under the assumption that the wave numbers are equal, one of the rolls must be aligned in the x-direction and the other one aligned in the y-direction.

THEOREM 4.2. *Assume that $I=(i_x,0,1)$ and $J=(0,j_y,1)$ ($i_x \geq 1$, $j_y \geq 1$) are the first critical indices with identical wave numbers, $\alpha_I = \alpha_J$. Consider the following numbers:*

$$\begin{aligned} b &= 2\kappa_{0,0,2}, \\ d &= 2\kappa_{0,0,2} + 8\kappa_{i_x,j_y,2}. \end{aligned} \tag{4.4}$$

For $R > R_c$, we define

$$\psi_i = g\sqrt{R-R_c}(X_i\phi_I + Y_i\phi_J) + o((R-R_c)^{1/2}), \quad i=1,\dots,8,$$

where

$$\begin{array}{llll} X_i=(-1)^i b^{-1/2}, & Y_i=0, & i=1,2, & \text{(roll pattern)} \\ X_i=0, & Y_i=(-1)^i b^{-1/2}, & i=3,4, & \text{(roll pattern)} \\ X_i=(b+d)^{-1/2}, & Y_i=(-1)^i X_i, & i=5,6, & \text{(mixed pattern)} \\ X_i=-(b+d)^{-1/2}, & Y_i=(-1)^i X_i, & i=7,8. & \text{(mixed pattern)} \end{array}$$

Then the topological structure of the system after the transition is as in figure 4.2. In particular,

1) Σ_R contains eight steady states ψ_i, $i=1,\dots,8$.
2) ψ_1, ψ_2, ψ_3, ψ_4 (rolls) are minimal attractors of Σ_R, whereas ψ_5, ψ_6, ψ_7, and ψ_8 (mixed) are unstable.
3) There is a neighborhood $\mathcal{U}\setminus\Gamma$ of 0, where Γ is the stable manifold of 0, such that $\bar{\mathcal{U}} = \cup_{i=1}^4 \bar{\mathcal{U}}_i$, with $\mathcal{U}_i$ pairwise disjoint, and where $\mathcal{U}_i$ is the basin of attraction of ψ_i, $i=1,\dots,4$.
4) The projection of $\mathcal{U}_i$ onto the space spanned by ϕ_I, ϕ_J is approximately a sectorial region given by

$$\mathcal{U}_i \cap \{X\phi_I + Y\phi_J \,|\, \omega_{i,1} < arg(X,Y) < \omega_{i,2}\}, \quad i=1,\dots,4,$$

$$\begin{array}{llll} \omega_{1,1}=3\pi/4, & \omega_{1,2}=5\pi/4, & \omega_{2,1}=-\pi/4, & \omega_{2,2}=\pi/4, \\ \omega_{3,1}=5\pi/4, & \omega_{3,2}=7\pi/4, & \omega_{4,1}=\pi/4, & \omega_{4,2}=3\pi/4. \end{array}$$

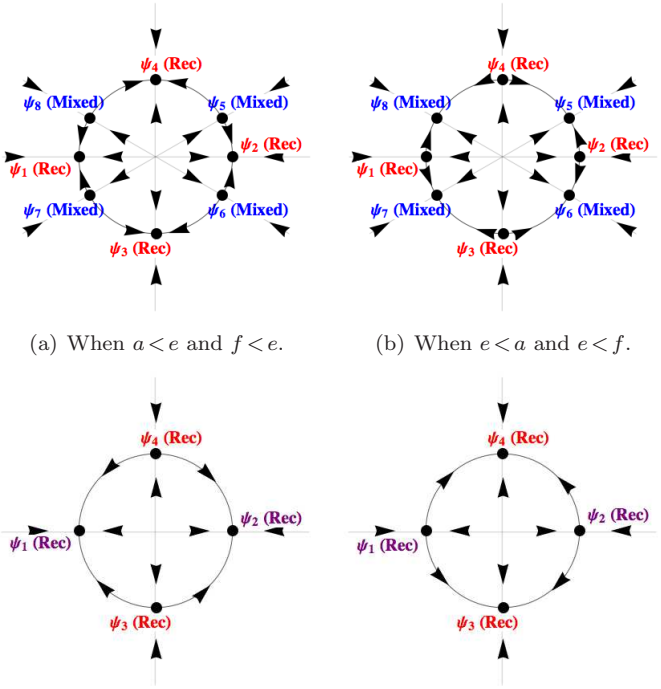

(a) When $a<e$ and $f<e$. (b) When $e<a$ and $e<f$.

(c) When $f<e<a$. (d) When $a<e<f$.

FIG. 4.4. *The structure of the attractor after the transition $R>R_c$ for different parameter regions, when the first two critical modes are both rectangle type.*

4.3. The first two critical modes are both rectangles. In this section we consider two critical modes both having a rectangular pattern with equal wave numbers, $\alpha_I=\alpha_J$.

THEOREM 4.3. *Assume that* $I=(i_x,i_y,1)$, $J=(j_x,j_y,1)$ $(i_x\neq 0,\ i_y\neq 0,\ j_x\neq 0,\ j_y\neq 0,\ i_x\neq j_x,\ i_y\neq j_y)$ are the first critical indices with identical wave numbers, $\alpha_I=\alpha_J$. Consider the following numbers:

$$\begin{aligned} a&=\kappa_{0,0,2}+\kappa_{2i_x,0,2}+\kappa_{0,2i_y,2},\\ e&=\kappa_{0,0,2}+\kappa_{i_x+j_x,i_y+j_y,2}+\kappa_{i_x-j_x,i_y+j_y,2}+\kappa_{i_x+j_x,-i_y+j_y,2}+\kappa_{i_x-j_x,-i_y+j_y,2},\\ f&=\kappa_{0,0,2}+\kappa_{2j_x,0,2}+\kappa_{0,2j_y,2}. \end{aligned} \tag{4.5}$$

For $R>R_c$, let us define the following steady state solutions:

$$\psi_i=g\sqrt{R-R_c}(X_i\phi_I+Y_i\phi_J)+o((R-R_c)^{1/2}),\quad i=1,\dots,8,$$

where

$$\begin{aligned} &X_i=(-1)^i a^{-1/2}, && Y_i=0, && i=1,2, && \text{(rectangle pattern)}\\ &X_i=0, && Y_i=(-1)^i f^{-1/2}, && i=3,4, && \text{(rectangle pattern)}\\ &X_i=\sqrt{\frac{e-f}{e^2-af}}, && Y_i=(-1)^i\sqrt{\frac{e-a}{2(e^2-af)}}, && i=5,6, && \text{(mixed pattern)} \end{aligned}$$

$$X_i = -\sqrt{\frac{e-f}{e^2-af}}, \quad Y_i = (-1)^i\sqrt{\frac{e-a}{2(e^2-af)}}, \qquad i=7,8. \qquad \text{(mixed pattern)}$$

There are four possible transition scenarios:

i) If $a<e$ and $f<e$ then the topological structure of the system after the transition is as in figure 4.4(a). In particular,
   1) Σ_R contains eight steady states ψ_i, $i=1,\ldots,8$.
   2) ψ_1, ψ_2, ψ_3, ψ_4 (rectangles) are minimal attractors of Σ_R, whereas ψ_5, ψ_6, ψ_7, and ψ_8 (mixed) are unstable.
   3) There is a neighborhood $\mathcal{U}\setminus\Gamma$ of 0, where Γ is the stable manifold of 0, such that $\bar{\mathcal{U}}=\cup_{i=1}^4\bar{\mathcal{U}}_i$, with $\mathcal{U}_i$ pairwise disjoint, and where $\mathcal{U}_i$ is the basin of attraction of ψ_i, $i=1,\ldots,4$.
   4) The projection of $\mathcal{U}_i$ onto the space spanned by ϕ_I, ϕ_J is approximately a sectorial region given by

$$\mathcal{U}_i\cap\{X\phi_I+Y\phi_J\,|\,\omega_{i,1}<arg(X,Y)<\omega_{i,2}\}, \quad i=1,\ldots,4,$$

$$\begin{aligned}
&\omega_{1,1}=\pi-\omega, \qquad &&\omega_{1,2}=\pi+\omega, \qquad &&\omega_{2,1}=-\omega, \qquad &&\omega_{2,2}=\omega,\\
&\omega_{3,1}=\pi+\omega, \qquad &&\omega_{3,2}=2\pi-\omega, \qquad &&\omega_{4,1}=\omega, \qquad &&\omega_{4,2}=\pi-\omega,
\end{aligned}$$

   where $\omega=\arctan\sqrt{\frac{e-a}{e-f}}$.

ii) If $e<a$ and $e<f$ then the topological structure of the system after the transition is as in figure 4.4(b). In particular,
   a) Σ_R contains eight steady states ψ_i, $i=1,\ldots,8$.
   b) ψ_5, ψ_6, ψ_7, ψ_8 (mixed) are minimal attractors of Σ_R, whereas ψ_1, ψ_2, ψ_3, ψ_4 (rectangles) are unstable.
   c) There is a neighborhood $\mathcal{U}\setminus\Gamma$ of 0, where Γ is the stable manifold of 0, such that $\bar{\mathcal{U}}=\cup_{i=5}^8\bar{\mathcal{U}}_i$, with $\mathcal{U}_i$ pairwise disjoint, and where $\mathcal{U}_i$ is the basin of attraction of ψ_i, $i=5,\ldots,8$.
   d) The projection of $\mathcal{U}_i$ onto the space spanned by ϕ_I, ϕ_J is a sectorial region given by

$$\mathcal{U}_i\cap\{X\phi_I+Y\phi_J\,|\,\omega_{i,1}<arg(X,Y)<\omega_{i,2}\}, \quad i=5,\ldots,8,$$

$$\begin{aligned}
&\omega_{5,1}=0, \qquad &&\omega_{5,2}=\pi/2, \qquad &&\omega_{6,1}=3\pi/2, \qquad &&\omega_{6,2}=2\pi,\\
&\omega_{7,1}=\pi, \qquad &&\omega_{7,2}=3\pi/2, \qquad &&\omega_{8,1}=\pi/2, \qquad &&\omega_{8,2}=\pi.
\end{aligned}$$

iii) If $f<e<a$ then the topological structure of the system after the transition is as in figure 4.4(c). In particular,
   a) Σ_R contains four steady states ψ_i, $i=1,\ldots,4$.
   b) ψ_1, ψ_2 (rectangles) are minimal attractors of Σ_R, whereas ψ_3, ψ_4 (rectangles) are unstable steady states.
   c) There is a neighborhood $\mathcal{U}\setminus\Gamma$ of 0, where Γ is the stable manifold of 0, such that $\bar{\mathcal{U}}=\cup_{i=1}^2\bar{\mathcal{U}}_i$, with $\mathcal{U}_i$ pairwise disjoint, and where $\mathcal{U}_i$ is the basin of attraction of ψ_i, $i=1,2$.

d) The projection of $\mathcal{U}_i$ onto the space spanned by ϕ_I, ϕ_J is a sectorial region given by

$$\mathcal{U}_i \cap \{X\phi_I + Y\phi_J \,|\, \omega_{i,1} < arg(X,Y) < \omega_{i,2}\}, \quad i=1,2,$$

$$\omega_{1,1} = \pi/2,\ \omega_{1,2} = 3\pi/2, \quad \omega_{2,1} = -\pi/2,\ \omega_{2,2} = \pi/2.$$

iv) If $a<e<f$ then the topological structure of the system after the transition is as in figure 4.4(d). In particular,

a) Σ_R contains four steady states ψ_i, $i=1,\ldots,4$.

b) ψ_3, ψ_4 (rectangles) are minimal attractors of Σ_R, whereas the ψ_1, ψ_2 (rectangles) are unstable steady states.

c) There is a neighborhood $\mathcal{U}\setminus\Gamma$ of 0, where Γ is the stable manifold of 0, such that $\bar{\mathcal{U}} = \cup_{i=3}^4 \bar{\mathcal{U}}_i$, with $\mathcal{U}_i$ pairwise disjoint, and where $\mathcal{U}_i$ is the basin of attraction of ψ_i, $i=3,4$.

d) The projection of $\mathcal{U}_i$ onto the space spanned by ϕ_I, ϕ_J is a sectorial region given by

$$\mathcal{U}_i \cap \{X\phi_I + Y\phi_J \,|\, \omega_{i,1} < arg(X,Y) < \omega_{i,2}\}, \quad i=3,4,$$

$$\omega_{3,1} = \pi,\ \omega_{3,2} = 2\pi, \quad \omega_{4,1} = 0,\ \omega_{4,2} = \pi.$$

5. Proof of the main theorems

First we give the preliminary setting that will be used in the proof of the main theorems.

The first step is to find the adjoint critical eigenvectors. The adjoint equation of (3.1) is

$$\begin{aligned} &\mathrm{Pr}(\Delta\mathbf{u}^* - \nabla p^*) + \theta^*\mathbf{k} = \bar{\beta}\mathbf{u}^*, \\ &\Delta\theta^* + R\,\mathrm{Pr}\, w^* = \bar{\beta}\theta^*, \\ &\mathrm{div}\mathbf{u}^* = 0. \end{aligned} \tag{5.1}$$

The eigenfunctions of (5.1) can be represented by the separation of variables (3.2). Also the eigenvalues of (5.1) are same as the eigenvalues of (3.1), i.e. $\bar{\beta}$ satisfies (3.5). We find the amplitudes of the critical adjoint eigenvectors as

$$W_S^* = \beta_S^1(R) + \gamma_S^2, \qquad \Theta_S^* = R\,\mathrm{Pr}, \tag{5.2}$$

where $\beta_S^1(R)$ satisfies the PES condition (3.8).

Let I and J be the indices of the critical modes, i.e. $\mathcal{C} = \{I, J\}$ in (3.8). We will denote

$$\phi_I = \phi_I^1, \quad \phi_J = \phi_J^1, \quad \beta(R) = \beta_I^1(R) = \beta_J^1(R).$$

To study the dynamics on the center manifold, we write:

$$\phi = \phi^c + \Phi(x,y),$$

in (2.5), where Φ is the center manifold function and

$$\phi^c = x\phi_I + y\phi_J.$$

Multiplying the governing evolution equation (2.5) by the adjoint eigenvectors ϕ_I^* and ϕ_J^*, we see that the amplitudes of the critical modes satisfy the following equations:

$$\begin{aligned}\frac{dx}{dt} &= \beta(R)x + \frac{1}{\langle \phi_I, \phi_I^* \rangle} \langle G(\phi), \phi_I^* \rangle, \\ \frac{dy}{dt} &= \beta(R)y + \frac{1}{\langle \phi_J, \phi_J^* \rangle} \langle G(\phi), \phi_J^* \rangle.\end{aligned} \tag{5.3}$$

The pairing $\langle \cdot, \cdot \rangle$ denotes the $L^2(\Omega)$ inner product.

By (3.8) and (3.5),

$$\beta(R) = g(R - R_c) + o((R - R_c)^2), \quad \text{as } R \to R_c, \tag{5.4}$$

with

$$g = \frac{d\beta}{dR}\Big|_{R=R_c} = \frac{\Pr \alpha^2}{(\Pr + 1)\gamma^4} \neq 0.$$

We write the phase space as

$$H = E_1 \oplus E_2, \qquad E_1 = \operatorname{span}\{\phi_I, \phi_J\}, \qquad E_2 = E_1^{\perp}.$$

As the linear part of (5.3) is diagonal, we have the following approximation of the center manifold (see Ma and Wang [8]):

$$-\mathcal{L}_R \Phi(x, y) = P_2 G(\phi^c) + o(2), \tag{5.5}$$

where $\mathcal{L}_R = L_R|_{E_2}$, P_2 is the projection onto E_2, and

$$o(n) = o(|(x, y)|^n) + O(|(x, y)|^n |\beta(R)|).$$

We know that the center manifold is tangent to E_1, so we have

$$\Phi(x, y) := \Phi_2(x, y) + o(2), \tag{5.6}$$

where $\Phi_2 \in E_2$ consists of quadratic terms. By direct computation we can show that there is no nonlinear interaction between the critical modes, i.e.

$$\langle G(\phi^c), \phi_K^* \rangle = \langle G(\phi^c, \phi^c), \phi_K^* \rangle = 0, \qquad K \in \mathcal{C}. \tag{5.7}$$

This implies that for $K \in \mathcal{C}$,

$$\begin{aligned}\langle G(\phi^c + \Phi), \phi_K^* \rangle &= \langle G(\phi^c, \Phi_2) + G(\Phi, \phi^c), \phi_K^* \rangle + o(3) \\ &= \langle G_s(\phi^c, \Phi_2), \phi_K^* \rangle + o(3).\end{aligned} \tag{5.8}$$

Here G_s is as defined by (2.6). By (5.6), (5.7), and the bilinearity of G, we can write (5.3) as

$$\begin{aligned}\frac{dx}{dt} &= \beta(R)x + p_I(x, y) + o(3), \\ \frac{dy}{dt} &= \beta(R)y + p_J(x, y) + o(3),\end{aligned} \tag{5.9}$$

where for $K \in \mathcal{C}$, $p_K(x,y)$ is a cubic polynomial given by

$$p_K(x,y) = \frac{1}{\langle \phi_K, \phi_K^* \rangle} \langle G_s(\phi^c, \Phi_2), \phi_K^* \rangle.$$

So to fully determine the reduced equation (5.9), we have to compute Φ_2 given by (5.6). In dynamic transition problems, the center manifold is generally expanded using the eigenfunctions of the original linear operator. However, following Sengul and Wang [13], we will expand the center manifold using a different basis. Namely we will consider the eigenfunctions $\mathbf{u}_S$ of the Stokes equation for the velocity together with eigenfunctions θ_S of the Laplace equation. The main advantage of such an expansion is that the eigenvalues and eigenfunctions are independent of the system parameters, namely the Prandtl number Pr and the Rayleigh number R, while still spanning the same functional space (2.3) which leads to computational advantages.

For this reason we turn to the following eigenvalue problem with the boundary conditions (2.2) of the original problem:

$$\begin{aligned} &\Delta \mathbf{u}_S - \nabla p = \rho \mathbf{u}_S, \\ &\Delta \theta_S = \rho \theta_S, \\ &\mathrm{div} \mathbf{u}_S = 0. \end{aligned}$$

By the classical theory of elliptic operators, the eigenvectors $\{e_S^1 = (\mathbf{u}_S, 0), e_S^2 = (0, \theta_S)\}$ form a basis of the phase space H. Moreover, e_S can be expressed by the same separation of variables (3.2). There are three cases to be considered.

- If $(s_x, s_y) = (0,0)$ and $s_z \neq 0$, then $e_S^1 = 0$ and
$$e_S^2 = (0, \theta_S), \qquad \Theta_S = 1.$$
- If $s_x^2 + s_y^2 \neq 0$ and $s_z = 0$, then there are eigenmodes which have the form $e = (\mathbf{u}, 0)$ with $\mathbf{u} = (u, v, 0)$. For such modes, it can be verified by direct computation that
$$\langle G(\phi^c), e \rangle = 0.$$
Thus by (5.5), such modes will not be present in the lowest order approximation of the center manifold function.
- If $s_x^2 + s_y^2 \neq 0$ and $s_z \neq 0$, then the multiplicity of an eigenvalue is two and the eigenvectors are
$$\begin{aligned} e_S^1 &= (\mathbf{u}_S, 0), \qquad W_S = 1, \\ e_S^2 &= (0, \theta_S), \qquad \Theta_S = 1. \end{aligned}$$

The following lemma is crucial in the computation of (5.5).

LEMMA 5.1. *For $i = 1,2$,*

$$\begin{aligned} &P_2 e_S^i = e_S^i && \text{for } S \notin \mathcal{C}, \\ &\langle P_2 G(\phi^c), e_S^i \rangle = 0 && \text{for } S \in \mathcal{C}. \end{aligned} \tag{5.10}$$

Proof. First note that

$$E_1 = \mathrm{span}\{\phi_I^1, \phi_J^1\} \subset \mathrm{span}\{e_S^1, e_S^2 \mid S \in \mathcal{C}\}.$$

Thus

$$E_2 = E_1^{\perp} \supset \operatorname{span}\{e_S^1, e_S^2 \mid S \notin \mathcal{C}\}.$$

Thus we have the first equation in (5.10).

Since

$$\operatorname{span}\{\phi_S^1, \phi_S^2 \mid S \in \mathcal{C}\} = \operatorname{span}\{e_S^1, e_S^2 \mid S \in \mathcal{C}\},$$

there must exist constants $c_{S,1} \neq 0$, $c_{S,2} \neq 0$ such that

$$P_2 e_S^1 = c_{S,1}\phi_S^2, \quad P_2 e_S^2 = c_{S,2}\phi_S^2, \quad \text{for } S \in \mathcal{C}.$$

Since by direct computation we have

$$\langle P_2 G(\phi^c), \phi_S^2 \rangle = 0, \quad \text{for } S \in \mathcal{C},$$

we also have second equation in (5.10). ∎

Now we write

$$\Phi_2 = \sum_{S \in \mathcal{S}, i=1,2} \Phi_S^i(x,y) e_S^i, \tag{5.11}$$

where $\mathcal{S}$ denotes some index set which will be specified later. Here Φ_S^i are quadratic polynomials in x and y. To find Φ_2 we need to compute Φ_S^i, which will be done in Lemma 5.2 and Lemma 5.3.

Let

$$\mathcal{Z}_\alpha^{roll} = \{K = (k,0,1) \text{ or } K = (0,k,1) : k \neq 0, \alpha_K = \alpha\},$$
$$\mathcal{Z}_\alpha^{rec} = \{K = (k_1,k_2,1) : k_1 \neq 0, k_2 \neq 0, \alpha_K = \alpha\}.$$

LEMMA 5.2. *For $S_1 = (0,0,2)$ we have*

$$\Phi_{S_1} = [\Phi_{S_1}^1, \Phi_{S_1}^2]^T = [0, \Phi_{S_1}^I x^2 + \Phi_{S_1}^J y^2]^T,$$

where for $K \in \{I,J\}$,

$$\Phi_{S_1}^K = \begin{cases} -\frac{\gamma^2}{16\pi}, & \text{if } K \in \mathcal{Z}_\alpha^{rec}, \\ -\frac{\gamma^2}{8\pi}, & \text{if } K \in \mathcal{Z}_\alpha^{roll}. \end{cases} \tag{5.12}$$

Also for $K_1 \in \mathcal{Z}_\alpha^{rec}, K_2 \in \mathcal{Z}_\alpha^{roll}$,

$$G_s(\phi_{K_1}, e_{S_1}, \phi_{K_1}^*) = \frac{1}{2} G_s(\phi_{K_2}, e_{S_1}, \phi_{K_2}^*) = \frac{L_1 L_2 \pi \gamma^2 R_c}{8} [0, \Pr]^T. \tag{5.13}$$

Proof. If $(s_x, s_y) = (0,0)$ and $s_z \neq 0$ then, by (5.5), for $K \in \{I,J\}$ we have

$$\Phi_S^K = \frac{\langle G(\phi_K, \phi_K), e_S^2 \rangle}{\langle e_S^2, \mathcal{L}_R^* e_S^2 \rangle} = \frac{\langle G(\phi_K, \phi_K), e_S^2 \rangle}{-s_z^2 \pi^2 \langle e_S^2, e_S^2 \rangle}. \tag{5.14}$$

Note that

$$\langle e_S^2, e_S^2 \rangle = \int_\Omega \sin^2 2\pi z = \frac{L_1 L_2}{2}. \tag{5.15}$$

For $K_1 \in \mathcal{Z}_\alpha^{rec}$, $K_2 \in \mathcal{Z}_\alpha^{roll}$, a direct computation yields

$$G(\phi_{K_1},\phi_{K_1},e_{S_1}) = \frac{1}{2}G(\phi_{K_2},\phi_{K_2},e_{S_1}) = \frac{-L_1L_2\pi\gamma^2}{8}[0,1]^T. \tag{5.16}$$

Here G_s is the trilinear operator defined in (2.6). Now, (5.12) follows from (5.14), (5.15), and (5.16). Also, (5.13) follows from an easy computation. ∎

LEMMA 5.3. *If $S \notin \mathcal{C}$, $S=(s_x,s_y,s_z)$, $(s_x,s_y)\neq(0,0)$, and $s_z\neq 0$, then*

$$\Phi_S = \begin{bmatrix} \Phi_S^1 \\ \Phi_S^2 \end{bmatrix} = -\frac{1}{\mathfrak{v}_S}\mathcal{A}_S{}^{-1}\begin{bmatrix} \langle G(\phi^c), e_S^1\rangle \\ \langle G(\phi^c), e_S^2\rangle \end{bmatrix}. \tag{5.17}$$

Here

$$\mathcal{A}_S = \begin{pmatrix} -\Pr\gamma_S^4\alpha_S^{-2} & R\Pr \\ 1 & -\gamma_S^2 \end{pmatrix} \tag{5.18}$$

and

$$\mathfrak{v}_S = \begin{cases} \dfrac{L_1L_2}{4}, \text{ if } (s_x,s_y)\neq(0,0), s_x=0 \text{ or } s_y=0, \\ \dfrac{L_1L_2}{8}, \text{ if } s_xs_y\neq 0, \end{cases} \tag{5.19}$$

Proof. Let

$$\mathcal{A}_S^{ij} = \frac{1}{\mathfrak{v}_S}\langle e_S^j, \mathcal{L}_R^* e_S^i\rangle, \qquad i,j=1,2, \tag{5.20}$$

that is,

$$\mathcal{A}_S = \frac{1}{\mathfrak{v}_S}\begin{pmatrix} \langle e_S^1,\mathcal{L}_R^*e_S^1\rangle & \langle e_S^2,\mathcal{L}_R^*e_S^1\rangle \\ \langle e_S^1,\mathcal{L}_R^*e_S^2\rangle & \langle e_S^2,\mathcal{L}_R^*e_S^2\rangle \end{pmatrix}.$$

Note that

$$\begin{aligned} &\langle e_S^1,e_S^1\rangle = \mathfrak{v}_S\frac{\gamma_S^2}{\alpha_S^2}, && \langle e_S^1,e_S^2\rangle = 0, \\ &\langle e_S^2,e_S^1\rangle = 0, && \langle e_S^2,e_S^2\rangle = \mathfrak{v}_S, \end{aligned} \tag{5.21}$$

where

$$\mathfrak{v}_S = \int_0^{L_1}\int_0^{L_2}\int_0^1 \cos^2\frac{s_x\pi x_1}{L_1}\cos^2\frac{s_y\pi x_2}{L_2}\cos^2 s_z\pi x_3.$$

Clearly $\mathfrak{v}_S$ is equal to the definition in (5.19). By (5.1), we have

$$\begin{aligned} &\mathcal{L}_R^*e_S^1 = (\Pr\Delta e_S^1 + R\Pr e_S^2), \\ &\mathcal{L}_R^*e_S^2 = (0,0,\cos(L_1^{-1}s_x\pi x)\cos(L_2^{-1}s_y\pi y)\sin(s_z\pi z),0) + \Delta e_S^2. \end{aligned} \tag{5.22}$$

Using the fact that $\Delta e_S^i = -\gamma_S^2$, $i=1,2$ and

$$\begin{aligned} &\langle e_S^1,(0,0,\cos(L_1^{-1}s_x\pi x)\cos(L_2^{-1}s_y\pi y)\sin(s_z\pi z),0)\rangle = \mathfrak{v}_S, \\ &\langle e_S^2,(0,0,\cos(L_1^{-1}s_x\pi x)\cos(L_2^{-1}s_y\pi y)\sin(s_z\pi z),0)\rangle = 0, \end{aligned}$$

it is easy to compute $\mathcal{A}_S$ by (5.20), (5.21), and (5.22), and show that it is indeed given by (5.18). Now we take the inner product of (5.5) by e_S^i, $i=1,2$. Writing

$$\Phi = \sum_K \Phi_K^1 e_K^1 + \Phi_K^2 e_K^2,$$

the inner product of left hand side of (5.5) by e_S^i becomes

$$\langle \mathcal{L}_R \Phi, e_S^i \rangle = \sum_K \sum_{j=1,2} \Phi_K^j \langle e_K^j, \mathcal{L}_R^* e_S^i \rangle = \sum_{j=1,2} \Phi_S^j \langle e_S^j, \mathcal{L}_R^* e_S^i \rangle = \mathfrak{v}_S \sum_{j=1,2} \mathcal{A}_S^{ij} \Phi_S^j. \tag{5.23}$$

For the inner product of e_S^i by the right hand side of (5.5) we use Lemma 5.1. This finishes the proof. ∎

Notice that

$$\det \mathcal{A}_S = \Pr(R_S - R),$$

where

$$R_S = \frac{\gamma_S^6}{\alpha_S^2}. \tag{5.24}$$

Since $R_S > R_c$ for $S \notin \mathcal{C}$, the determinant of $\mathcal{A}$ is always positive when R is close to R_c. This guarantees that (5.17) can be solved for Φ_S^1 and Φ_S^2.

Finally note that if $S=(s_x,s_y,s_z)$ is a critical index with $(s_x,s_y)\neq(0,0)$ and $s_z\neq 0$ at $R=R_c$ we have

$$\begin{aligned}
\langle \phi_S, \phi_S^* \rangle &= \int_\Omega u_S u_S^* + v_S v_S^* + w_S w_S^* + \theta_S \theta_S^* \\
&= \mathfrak{v}_S \left(\left(\frac{s_z^2 \pi^2}{\alpha_S^2} + 1 \right) W_S W_S^* + \Theta_S \Theta_S^* \right) \\
&= \mathfrak{v}_S \left(\frac{\gamma_S^2}{\alpha_S^2} (\gamma_S^2 + \beta(R))^2 + R \Pr \right) \Big|_{R=R_c} \\
&= \mathfrak{v}_S (\Pr + 1) R_c.
\end{aligned} \tag{5.25}$$

NOTATION 5.1. *We will use the following notation:*

$$G(\phi_I, \phi_J, e_S) = \begin{bmatrix} G(\phi_I, \phi_J, e_S^1) \\ G(\phi_I, \phi_J, e_S^2) \end{bmatrix}.$$

We also define the following indices, which will be used throughout the proofs:

$$\begin{aligned}
&S_1 = (0,0,2), S_2 = (2i_x,0,2), S_3 = (0,2i_y,2), S_4 = (i_x, i_y + j_y, 2), \\
&S_5 = (i_x, j_y - i_y, 2), S_6 = (i_x, j_y, 2), S_7 = (i_x + j_x, i_y + j_y, 2), \\
&S_8 = (i_x - j_x, i_y + j_y, 2), S_9 = (i_x + j_x, -i_y + j_y, 2), \\
&S_{10} = (i_x - j_x, -i_y + j_y, 2), S_{11} = (2j_x, 0, 2), S_{12} = (0, 2j_y, 2).
\end{aligned} \tag{5.26}$$

5.1. Proof of Theorem 4.1. Assume that $I=(i_x,i_y,1)$ and $J=(0,j_y,1)$, $(i_x\geq 1,\ j_y>i_y\geq 1)$ are the first critical indices with identical wave numbers, $\alpha_I=\alpha_J$. Using (5.5), we find that the lowest order approximation of the center manifold is spanned by the eigenvectors having indices S_i as given in (5.26):

$$\Phi(x,y)=x^2(\Phi^I_{S_1}e_{S_1}+\sum_{S=S_2,S_3}\Phi_S e_S)+xy\sum_{S=S_4,S_5}\Phi_S e_S+y^2\Phi^J_{S_1}e_{S_1}.$$

Here

$$\Phi_{S_1}=x^2\Phi^I_{S_1}+y^2\Phi^J_{S_1},$$

where according to (5.12) we have

$$\Phi^J_{S_1}=2\Phi^I_{S_1}.$$

The cubic polynomials in (5.9) are as follows:

$$\begin{aligned}
&p_I=x(a_1x^2+a_2y^2),\quad p_J=y(b_1x^2+b_2y^2),\\
&a_1=\frac{1}{\langle\phi_I,\phi_I^*\rangle}\left(\Phi^I_{S_1}G_s(\phi_I,e_{S_1},\phi_I^*)+\sum_{i=2,3}\Phi_{S_i}G_s(\phi_I,e_{S_i},\phi_I^*)\right),\\
&a_2=\frac{1}{\langle\phi_I,\phi_I^*\rangle}\left(\Phi^J_{S_1}G_s(\phi_I,e_{S_1},\phi_I^*)+\sum_{i=4,5}\Phi_{S_i}G_s(\phi_J,e_{S_i},\phi_I^*)\right),\\
&b_1=\frac{1}{\langle\phi_J,\phi_J^*\rangle}\left(\Phi^I_{S_1}G_s(\phi_J,e_{S_1},\phi_J^*)+\sum_{i=4,5}\Phi_{S_i}G_s(\phi_I,e_{S_i},\phi_J^*)\right),\\
&b_2=\frac{1}{\langle\phi_J,\phi_J^*\rangle}\Phi^J_{S_1}G_s(\phi_J,e_{S_1},\phi_J^*).
\end{aligned}\tag{5.27}$$

As evident from the formulas (5.17) and (5.27), an important part of the proof is a careful calculation of the nonlinear interactions between the set of critical modes and the set of resonant modes with the wave numbers given by (5.26). This involves the exact calculation of dozens if not hundreds of triple integrals of the form (2.6). For this purpose, we used the symbolic integration capabilities of Mathematica.

All the terms involving S_1 above can be computed using the Lemma 5.2. By direct computation,

$$G_s(\phi_I,e_S,\phi_J^*)=G_s(\phi_J,e_S,\phi_I^*),\quad S=S_4,S_5.\tag{5.28}$$

Putting (5.12), (5.28), and (5.25) into (5.27) we find that

$$a_2=2b_1.\tag{5.29}$$

By direct computation we can obtain the following:

$$\begin{aligned}
&G(\phi_I,\phi_I,e_S)=-\frac{1}{2}\eta_S\begin{bmatrix}\alpha^{-2}\\ \gamma^{-4}\end{bmatrix},\quad S=S_2,S_3,\\
&G_s(\phi_I,\phi_J,e_S)=-\eta_S\begin{bmatrix}\alpha^{-2}\\ \gamma^{-4}\end{bmatrix},\quad S=S_4,S_5,
\end{aligned}\tag{5.30}$$

$$\begin{aligned} G_s(\phi_I, e_S, \phi_I^*) &= \frac{1}{2}\eta_S \begin{bmatrix} \alpha^{-2} \\ \Pr R_c \gamma^{-4} \end{bmatrix}, \quad S = S_2, S_3, \\ G_s(\phi_J, e_S, \phi_I^*) &= \frac{1}{2}\eta_S \begin{bmatrix} \alpha^{-2} \\ \Pr R_c \gamma^{-4} \end{bmatrix}, \quad S = S_4, S_5, \end{aligned} \tag{5.31}$$

where

$$\eta_S = \frac{L_1 L_2 \pi (4\alpha^2 - \alpha_S^2)\gamma^6}{32\alpha^2}. \tag{5.32}$$

Using (5.14), (5.17), and (5.30), we find

$$\begin{aligned} \Phi_S = \begin{bmatrix} \Phi_S^1 \\ \Phi_S^2 \end{bmatrix} &= \frac{1}{16}\frac{\pi(4\alpha^2 - \alpha_S^2)\gamma^2}{\Pr \alpha^4 (R_c - R_S)} \begin{bmatrix} \Pr R_c \alpha^2 + \gamma^4 \gamma_S^2 \\ \Pr \frac{R_S}{\gamma_S^2} \alpha^2 + \gamma^4 \end{bmatrix}, \quad S = S_2, S_3, \\ \Phi_S = \begin{bmatrix} \Phi_S^1 \\ \Phi_S^2 \end{bmatrix} &= \frac{1}{4}\frac{\pi(4\alpha^2 - \alpha_S^2)\gamma^2}{\Pr \alpha^4 (R_c - R_S)} \begin{bmatrix} \Pr R_c \alpha^2 + \gamma^4 \gamma_S^2 \\ \Pr \frac{R_S}{\gamma_S^2} \alpha^2 + \gamma^4 \end{bmatrix}, \quad S = S_4, S_5. \end{aligned} \tag{5.33}$$

Now putting (5.31), (5.33), (5.16), (5.12) into (5.27), using (5.29), the equation (5.9) becomes

$$\begin{aligned} \frac{dx}{dt} &= \beta(R)x - x(ax^2 + 2cy^2) + o(3), \\ \frac{dy}{dt} &= \beta(R)y - y(cx^2 + 2by^2) + o(3), \end{aligned} \tag{5.34}$$

where a, b, and c are as defined in (4.2). Note also that $\kappa_{S_i} > 0$ in (4.1) since $R_c < R_{S_i}$, $i = 1, \ldots, 5$ and we have the following relations:

$$0 < b < a, \quad 0 < b < c. \tag{5.35}$$

Now we consider the approximate steady state equations of (5.34):

$$\begin{aligned} \beta(R)x - x(ax^2 + 2cy^2) &= 0, \\ \beta(R)y - y(cx^2 + 2by^2) &= 0. \end{aligned} \tag{5.36}$$

Let us define

$$\omega^2 := \frac{c - a}{2(c - b)}. \tag{5.37}$$

There are two cases to consider.

i) If $c < a$, then the equations (5.36) have only four straight line orbits on the lines $y = 0$ and $x = 0$. And the following solutions of (5.36) are bifurcated on $\beta > 0$:

$$X_\pm = \left(\pm\sqrt{\frac{\beta}{a}}, 0 \right), \quad Y_\pm = \left(0, \pm\sqrt{\frac{\beta}{2b}} \right). \tag{5.38}$$

ii) If $c > a$ then there are four additional straight line orbits on the lines $y = \pm\omega x$. Note that in this case, by (5.35), $c^2 - ab > 0$ and there are four additional solutions bifurcated on $\beta > 0$ which are given by

$$Z_\pm^i = (-1)^i (1, \pm\omega) \sqrt{\beta \frac{c - b}{c^2 - ab}}, \quad i = 1, 2. \tag{5.39}$$

Now the Jacobian of the vector field in (5.36) is

$$J=\begin{pmatrix}\beta-3ax^2-2cy^2 & -4cyx\\ -2cyx & \beta-cx^2-6by^2\end{pmatrix}. \tag{5.40}$$

The Jordan canonical forms of the Jacobian matrix evaluated at the steady states in (5.38) and (5.39) are as follows:

$$\begin{aligned}&J(X_\pm)=2\beta\begin{pmatrix}-1 & 0\\ 0 & \frac{a-c}{2a}\end{pmatrix},\quad J(Y_\pm)=2\beta\begin{pmatrix}\frac{b-c}{2b} & 0\\ 0 & -1\end{pmatrix},\\ &J(Z^i_\pm)\sim 2\beta\begin{pmatrix}-1 & 0\\ 0 & \frac{(b-c)(c-a)}{ab-c^2}\end{pmatrix},\quad i=1,2.\end{aligned} \tag{5.41}$$

The stability of the steady states can be found by using (5.41). Since $c>b$, $Y_\pm$ are always stable on $R>R_c$. If $c>a$ then $X_\pm$ are stable and $Z_\pm$ are unstable on $R>R_c$. On the other hand if $c<a$ then $X_\pm$ are unstable and $Z_\pm$ are not bifurcated on $R>R_c$. Thus we have two transition scenarios and the results are shown in figure 4.2.

REMARK 5.1. In the particular case $j_y=2i_y$, the equations in (5.34) can be reduced further. In this case we have $\alpha_{S_2}=\alpha_{S_4}$ and $\alpha_{S_3}=\alpha_{S_5}$, which implies that $\gamma_{S_2}=\gamma_{S_4}$ and $\gamma_{S_3}=\gamma_{S_5}$. This in turn implies $\kappa_{S_2}=\kappa_{S_4}$ and $\kappa_{S_3}=\kappa_{S_5}$, and we get the relation $2a=b+c$. This implies $c>a$ since $c-a=a-b>0$.

5.2. Proof of Theorem 4.2. We point out the differences from the previous proof. We have $I=(i_x,0,1)$ and $J=(0,j_y,1)$ ($i_x\geq 1$, $j_y\geq 1$) as the first critical indices with identical wave numbers, $\alpha_I=\alpha_J$. First, the center manifold is given by

$$\Phi(x,y)=x^2\Phi^I_{S_1}\phi_{S_1}+xy\Phi_{S_6}e_{S_6}+y^2\Phi^J_{S_1}e_{S_1}+o(2).$$

Using this approximation, the cubic polynomials in (5.9) are as follows:

$$\begin{aligned}&p_I=x(a_1x^2+a_2y^2),\quad p_J=y(b_1x^2+b_2y^2),\\ &a_1=\frac{1}{\langle\phi_I,\phi^*_I\rangle}\Phi^I_{S_1}G_s(\phi_I,e_{S_1},\phi^*_I),\\ &a_2=\frac{1}{\langle\phi_I,\phi^*_I\rangle}\left(\Phi^J_{S_1}G_s(\phi_I,e_{S_1},\phi^*_I)+\Phi_{S_6}G_s(\phi_J,e_{S_6},\phi^*_I)\right),\\ &b_1=\frac{1}{\langle\phi_J,\phi^*_J\rangle}\left(\Phi^I_{S_1}G_s(\phi_J,e_{S_1},\phi^*_J)+\Phi_{S_6}G_s(\phi_I,e_{S_6},\phi^*_J)\right),\\ &b_2=\frac{1}{\langle\phi_J,\phi^*_J\rangle}\Phi^J_{S_1}G_s(\phi_J,e_{S_1},\phi^*_J).\end{aligned} \tag{5.42}$$

The coefficients a_1 and b_2 are equal to b_2 in the proof of the first theorem. Thus we only need to find a_2 and b_1. A quick computation shows that

$$G_s(\phi_I,e_{S_6},\phi^*_J)=G_s(\phi_J,e_{S_6},\phi^*_I), \tag{5.43}$$

which shows that

$$a_2=b_1. \tag{5.44}$$

By direct computation we can obtain the following:

$$G_s(\phi_I,\phi_J,e_S)=-2\eta_S\begin{bmatrix}\alpha^{-2}\\ \gamma^{-4}\end{bmatrix},\quad S=S_6, \tag{5.45}$$

$$G_s(\phi_J, e_S, \phi_I^*) = \eta_S \begin{bmatrix} \alpha^{-2} \\ \Pr R_c \gamma^{-4} \end{bmatrix}, \quad S = S_6, \tag{5.46}$$

where η is given by (5.32). Using (5.14), (5.17), and (5.45), we find

$$\Phi_S = \begin{bmatrix} \Phi_S^1 \\ \Phi_S^2 \end{bmatrix} = \frac{1}{2} \frac{\pi(4\alpha^2 - \alpha_S^2)\gamma^2}{\Pr \alpha^4 (R_c - R_S)} \begin{bmatrix} \Pr R_c \alpha^2 + \gamma^4 \gamma_S^2 \\ \Pr \frac{R_S}{\gamma_S^2} \alpha^2 + \gamma^4 \end{bmatrix}, \quad S = S_6. \tag{5.47}$$

Using (5.44), the equations (5.9) become:

$$\begin{aligned} \frac{dx}{dt} &= \beta(R)x - x(bx^2 + dy^2) + o(3), \\ \frac{dy}{dt} &= \beta(R)y - y(dx^2 + by^2) + o(3). \end{aligned} \tag{5.48}$$

Here $b > 0$ and $d > 0$ are defined in (4.4). Since $\kappa > 0$, we always have $b < d$. Now we consider the approximate steady state equations of (5.48):

$$\begin{aligned} \beta(R)x - x(bx^2 + dy^2) &= 0, \\ \beta(R)y - y(dx^2 + by^2) &= 0. \end{aligned} \tag{5.49}$$

The equations (5.49) have always eight straight line orbits on the lines $y = 0$, $x = 0$, and $y = \pm x$. The eight solutions of (5.49) which are bifurcated on $\beta > 0$ are

$$\begin{aligned} &X_\pm = \Big(\pm \sqrt{\frac{\beta}{b}}, 0 \Big), \quad Y_\pm = \Big(0, \pm \sqrt{\frac{\beta}{b}} \Big), \\ &Z_\pm^i = (-1)^i (1, \pm 1) \sqrt{\frac{\beta}{b+d}}, \quad i = 1,2. \end{aligned} \tag{5.50}$$

The Jordan canonical forms of the Jacobian matrix evaluated at the steady states in (5.50) are as follows:

$$\begin{aligned} &J(X_\pm) = 2\beta \begin{pmatrix} -1 & 0 \\ 0 & \frac{b-d}{2b} \end{pmatrix}, \quad J(Y_\pm) = 2\beta \begin{pmatrix} \frac{b-d}{2b} & 0 \\ 0 & -1 \end{pmatrix}, \\ &J(Z_\pm^i) \sim 2\beta \begin{pmatrix} -1 & 0 \\ 0 & \frac{d-b}{d+b} \end{pmatrix}, \quad i = 1,2. \end{aligned} \tag{5.51}$$

Using (5.51) we can find that, since $b < d$, $X_\pm$ and $Y_\pm$ are stable and $Z_\pm^i$, $i = 1,2$ are unstable on $R > R_c$. That finishes the proof.

5.3. Proof of Theorem 4.3. Again we point out the differences from the previous proofs. We have $I = (i_x, i_y, 1)$, $J = (j_x, j_y, 1)$ $(i_x \neq 0,\ i_y \neq 0,\ j_x \neq 0,\ j_y \neq 0)$ as the first critical indices with identical wave numbers, $\alpha_I = \alpha_J$. First, the center manifold is given by

$$\begin{aligned} \Phi(x,y) = {} & x^2 (\Phi_{S_1}^I \phi_{S_1} + \sum_{S = S_2, S_3} \Phi_S e_S) + xy \sum_{S = S_7, S_8, S_9, S_{10}} \Phi_S e_S \\ & + y^2 (\Phi_{S_1}^J \phi_{S_1} + \sum_{S = S_2, S_3} \Phi_S e_S) + o(2). \end{aligned}$$

Using this approximation, the cubic polynomials in (5.9) are as follows:

$$\begin{aligned}
&p_I = x(a_1x^2 + a_2y^2), \quad p_J = y(b_1x^2 + b_2y^2),\\
&a_1 = \frac{1}{\langle \phi_I, \phi_I^* \rangle}(\Phi^I_{S_1} G_s(\phi_I, e_{S_1}, \phi_I^*) + \sum_{i=2,3} \Phi_{S_i} G_s(\phi_I, e_{S_i}, \phi_I^*)),\\
&a_2 = \frac{1}{\langle \phi_I, \phi_I^* \rangle}(\Phi^J_{S_1} G_s(\phi_I, e_{S_1}, \phi_I^*) + \sum_{i=7,\ldots,10} \Phi_{S_i} G_s(\phi_J, e_{S_i}, \phi_I^*)),\\
&b_1 = \frac{1}{\langle \phi_J, \phi_J^* \rangle}(\Phi^I_{S_1} G_s(\phi_J, e_{S_1}, \phi_J^*) + \sum_{i=7,\ldots,10} \Phi_{S_i} G_s(\phi_I, e_{S_i}, \phi_J^*)),\\
&b_2 = \frac{1}{\langle \phi_J, \phi_J^* \rangle}(\Phi^J_{S_1} G_s(\phi_J, e_{S_1}, \phi_J^*) + \sum_{i=11,12} \Phi_{S_i} G_s(\phi_J, e_{S_i}, \phi_J^*)).
\end{aligned} \tag{5.52}$$

a_1 and b_2 are computed in the same way as a_1 in the proof of the first theorem. So we need only find a_2 and b_1. Also using

$$G_s(\phi_I, e_S, \phi_J^*) = G_s(\phi_J, e_S, \phi_I^*), \quad S = S_7, S_8, S_9, S_{10}, \tag{5.53}$$

we find that

$$a_2 = b_1. \tag{5.54}$$

By direct computation we can obtain the following:

$$G_s(\phi_I, \phi_J, e_S) = -\frac{1}{2}\eta_S \begin{bmatrix} \alpha^{-2} \\ \gamma^{-4} \end{bmatrix}, \quad S = S_7, S_8, S_9, S_{10}, \tag{5.55}$$

$$G_s(\phi_J, e_S, \phi_I^*) = \frac{1}{4}\eta_S \begin{bmatrix} \alpha^{-2} \\ \Pr R_c \gamma^{-4} \end{bmatrix}, \quad S = S_7, S_8, S_9, S_{10}. \tag{5.56}$$

where η is given by (5.32). Using (5.14), (5.17), and (5.55), we find

$$\Phi_S = \begin{bmatrix} \Phi_S^1 \\ \Phi_S^2 \end{bmatrix} = \frac{1}{8}\frac{\pi(4\alpha^2 - \alpha_S^2)\gamma^2}{\Pr \alpha^4 (R_c - R_S)} \begin{bmatrix} \Pr R_c \alpha^2 + \gamma^4 \gamma_S^2 \\ \Pr \frac{R_S}{\gamma_S^2}\alpha^2 + \gamma^4 \end{bmatrix}, \quad S = S_7, S_8, S_9, S_{10}. \tag{5.57}$$

Using (5.54), the equations (5.9) become

$$\begin{aligned}
\frac{dx}{dt} &= \beta(R)x - x(ax^2 + ey^2) + o(3),\\
\frac{dy}{dt} &= \beta(R)y - y(ex^2 + fy^2) + o(3).
\end{aligned} \tag{5.58}$$

Here a, e, and f are positive numbers defined in (4.5).

Now we consider the approximate steady state equations of (5.58):

$$\begin{aligned}
\beta(R)x - x(ax^2 + ey^2) &= 0,\\
\beta(R)y - y(ex^2 + fy^2) &= 0.
\end{aligned} \tag{5.59}$$

The analysis of the equations (5.59) is similar to the analysis of the equations (5.36) given in the proof of Theorem 4.1. Thus we omit the details.

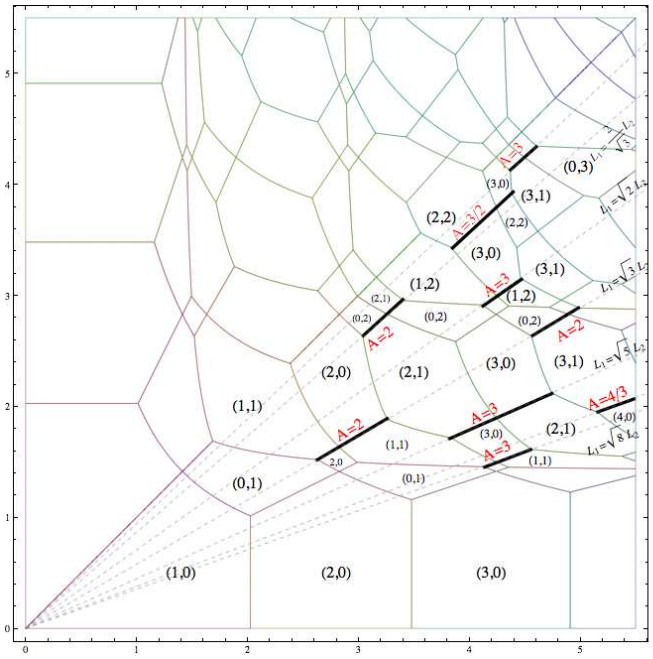

FIG. 6.1. *The selection of the horizontal wave indices* (i_x, i_y).

6. Physical remarks

In this section we will use the main theorems to derive some physical conclusions.

Before going into details, we have to make a remark about the critical wave number α since it is one of the parameters determining the transition numbers. Although α depends on the length scales, thanks to Lemma 3.1, we have certain bounds on its range of values. To recall, these are:

i) $\alpha > 1.55$ regardless of the length scale.

ii) If one of the length scales is greater than 2.03 then $\alpha < 3.10$.

Taking a look into figure 3.3, one sees that the only case which is not covered by taking α in the range $1.55 < \alpha < 3.10$ is that of two critical rolls with indices $I = (1,0,1)$ and $J = (0,1,1)$, which happens when $L_1 = L_2 < 1.69$.

There are only three possible cases when two modes with equal wave numbers become unstable simultaneously. Namely these two critical modes can be a rectangular and a roll mode, both roll modes, or both rectangular modes. We investigate each case separately.

6.1. The first two critical modes are a roll and a rectangle. We first consider two critical wave indices $I = (i_x, i_y, 1)$ of a rectangular pattern and $J = (0, j_y, 1)$ of a roll pattern with equal wave numbers $\alpha = \alpha_I = \alpha_J$; see figure 3.2. We define the following number:

$$A = \frac{j_y}{i_y}.$$

Since we are assuming that $\alpha_I = \alpha_J$, we have $1 \le i_y < j_y$ and $A > 1$. Notice that A is the ratio of the number of rolls to the number of the rectangle columns in the

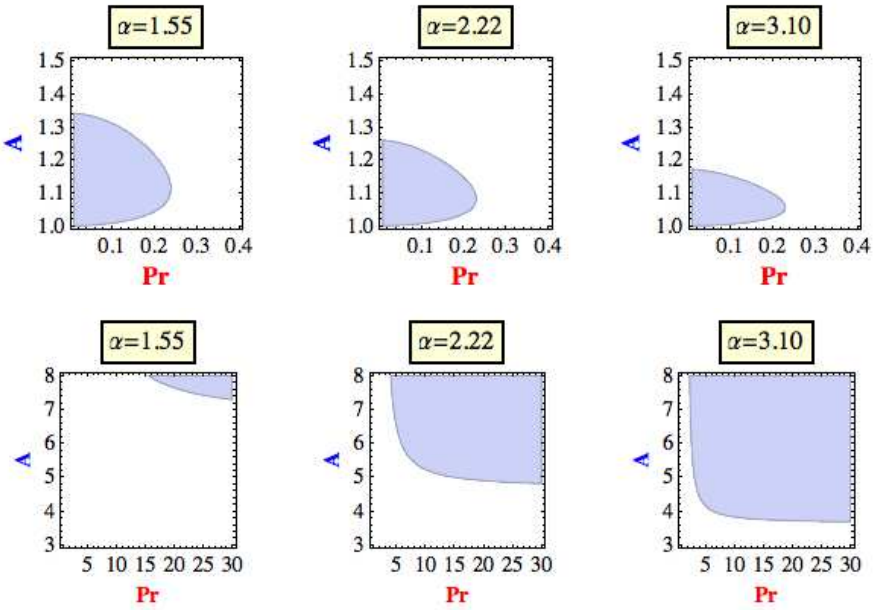

FIG. 6.2. *The shaded regions show the parameter regimes where $c<a$ when two critical indices are $I=(i_x,i_y,1)$ and $J=(0,j_y,1)$. Here $A=j_y/i_y$.*

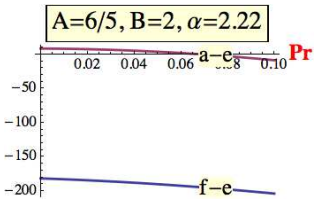

FIG. 6.3. *The parameters $a-e$ and $f-e$ in the small Prandtl number regime.*

direction of rolls. Figure 6.1 shows that the possible values of A in the small length scale regime $\max\{L_1,L_2\}<5.5$ are 4/3, 3/2, 2, 3, 4.

Now to use Theorem 4.1 to describe the pattern selection after the transition, we have to compute the transition numbers a and c given by (4.2). These numbers depend on three parameters Pr, L_1, and L_2. Equivalently one can use Pr, A, and α as the parameters determining a, b, and c.

Using

$$\alpha_{S_2}=2\sqrt{\alpha^2-\frac{\alpha^2}{A^2}},\quad \alpha_{S_3}=2\frac{\alpha}{A},\quad \alpha_{S_4}=\sqrt{2\alpha\Big(\alpha+\frac{\alpha}{A}\Big)},\quad \alpha_{S_5}=\sqrt{2\alpha\Big(\alpha-\frac{\alpha}{A}\Big)},$$

in (4.2), we can compute the numerical values of a and c for a given value of A, α, and Pr.

There are two possible cases, depending on whether $a<c$ or $c<a$. In figure 6.2, the regions where $c<a$ is shown for several parameter regimes. The results show that both transition scenarios described by Theorem 2.1 are possible. In particular there

are two parameter regimes such that $c<a$, namely when $\mathrm{Pr}<0.2$ and $1<A<1.4$ and for large A or large Pr.

Now some remarks are in order about the basin of attraction of the rolls and rectangles. When $a<c$, both rectangles and rolls are stable but their basins of attraction, which are sectorial regions, depend on an angle ω which depends on Pr, α, and A. In the particular case $A=2$, the mixed modes have a hexagonal pattern and we find that $a<c$. Moreover, ω is independent of α and Pr and is found to be $\omega=\arctan 1/2\approx 26.57^\circ$. So in this case the basin of attraction of rolls consists of two sectors each of which has an angle of $\pi-2\omega\approx 126.87^\circ$ while the basin for the rectangles have an angle of $2\omega\approx 53.13^\circ$. This means that rolls will attract a wider region of initial conditions than rectangles do.

6.2. The first two critical modes are both rolls. Now we consider two roll type critical modes. By the assumption of equal wave numbers, the rolls must be perpendicular to each other, i.e. $I=(i_x,0,1)$ and $J=(0,j_y,1)$. In this case after the first dynamic transition, the rolls are always stable and the mixed states are always unstable. Moreover, rolls with index I and rolls with index J have uniform attraction basins.

6.3. The first two critical modes are both rectangles. Now we consider the case where the first two critical modes both have rectangle patterns, i.e. $I=(i_x,i_y,1)$ and $J=(j_x,j_y,1)$ $(i_x>j_x\geq 1,\ j_y>i_y\geq 1)$ are the first critical wave indices. In this case, the dynamic transitions depend on the numbers a, e, and f given by Theorem 4.3. To calculate these numbers we define the parameters A and B:

$$A=\frac{j_y}{i_y}>1,\quad B=\frac{i_x}{j_x}>1.$$

Using the definition, we find that

$$\begin{aligned}
&\alpha^2_{2i_x,0}=4\frac{B^2(A^2-1)}{B^2A^2-1}\alpha^2,\quad \alpha^2_{0,2i_y}=4\frac{B^2-1}{B^2A^2-1}\alpha^2,\\
&\alpha^2_{2j_x,0}=4\frac{A^2(B^2-1)}{B^2A^2-1}\alpha^2,\quad \alpha^2_{0,2j_y}=4\frac{A^2-1}{B^2A^2-1}\alpha^2,\\
&\alpha^2_{i_x+(-1)^m j_x,(-1)^n i_y+j_y}=2\left(\alpha^2+\frac{(-1)^m}{4B}\alpha^2_{2i_x,0}+A\frac{(-1)^n}{4}\alpha^2_{0,2i_y}\right),\quad m,n=1,2.
\end{aligned}$$

Using this, we computed a, e, and f for several choices of Pr, α, B, and C. Our numerical calculations revealed that $a<e$ and $f<e$ for a vast amount of parameter choices. This means that the transition scenario is described in figure 4.4(a). Then the rectangles with index I and J are both stable and the mixed modes are unstable.

However, the other transition scenarios can also be possible, as we observed that $f<e<a$ when the Prandtl number is small, one of A or B is less than 2, and $A\neq B$. For an example see figure 6.3. In this case the transition scenario is described in figure 4.4(c). Hence only rectangles with index I are stable and the rectangles with index J are unstable.

In particular, our numerical investigations suggest that one or both of the pure modes (rectangles) are stable while the mixed modes are unstable.

The physical conclusions described by our theorems are in agreement with the previous experimental and theoretical results. It has been predicted that for the Boussinesq system driven solely by buoyancy, the mixed solutions are not stable after the first transition and the stability of mixed modes, such as hexagons, after the

transition is linked to a multitude of other factors such as the existence of temperature dependent surface tension or temperature-dependent viscosity or time dependent heating; see Busse [1], Getling [5], Koschmieder [6], Lappa [7], Palm [11], and Sengul & Wang [12]. However, we also note here that the mixed solutions are saddles which are connected to the stable steady states by heteroclinic orbits. Thus if the initial conditions are close to the mixed states at the onset of the convection, these mixed states will still be observable as transients, although in the long run the system will tend to the stable states.

7. Conclusions

In this paper, we discuss the dynamic transitions of Rayleigh-Bénard (RB) convection from a perspective of pattern formation. We focus on the case when two eigenvalues cross the imaginary axis simultaneously. This allows us to compare the stability of a pattern with respect to perturbations of other pattern types. Our main assumption is that the wave numbers of the critical modes are equal. Under this assumption, we classify all the possible transition scenarios and determine in each case the preferred patterns and their basins of attraction depending on the system parameters.

The pattern of a simple critical mode is either a rectangle or a roll. Thus there are three possible cases when there are two critical modes: (a) one mode is rectangular, the other mode is a roll, (b) both modes are rolls, (c) both modes are rectangles.

The following are some general characteristics of the transition for the RB convection which are already known (Ma and Wang [9, 10]):

1) The transition is Type-I. In particular, there is an attractor Σ_R bifurcating on $R > R_c$.
2) Σ_R is homeomorphic to S^1, and comprises the steady states and their connecting heteroclinic orbits.

The following are the results due to our main theorems:

3) In all the scenarios, we found that only pure modes (rolls or rectangles) are stable and the mixed modes are unstable. Our result is conclusive (analytical proof) when one of the critical modes is a roll type. When both critical modes are rectangles, we only have computational evidence.
4) When both critical modes are rolls, the stable steady states after the transition are rolls. When both critical modes are rectangles, computational evidence suggests that the stable steady states after the transition are rectangles. When one critical mode is a roll and the other one is a rectangle, the stable states after the transition can be either only rolls or both rolls and rectangles.
5) When both rolls and rectangles are stable after the transition, these states have non-uniform sectorial basin of attractions. In the particular case, where the mixed states have a regular hexagonal pattern, the angle of the sector for rolls is 126.87° while the angle of the sector for the rectangles is 53.13°. Thus rolls attract a wider range of initial conditions, making them a more preferable type of pattern.

Acknowledgment. The authors would like to thank an anonymous referee for his/her insightful comments.

REFERENCES

[1] F.H. Busse, *Non-linear properties of thermal convection*, Reports on Progress in Physics, 41, 1929–1967, 1978.

[2] S. Chandrasekhar, *Hydrodynamic and Hydromagnetic Stability*, International Series of Monographs on Physics, Dover Publications, 1981.

[3] M.C. Cross and P.C. Hohenberg, *Pattern formation outside of equilibrium*, Rev. Mod. Phys., 65(3), 851–1112, 1993.

[4] C. Foias, O. Manley, and R. Temam, *Attractors for the Bénard problem: Existence and physical bounds on their fractal dimension*, Nonlin. Anal., 11(8), 939–967, 1987.

[5] A.V. Getling, *Rayleigh-Bénard Convection: Structures and Dynamics*, Advanced Series in Nonlinear Dynamics, World Scientific, 1997.

[6] E.L. Koschmieder, *Bénard Cells and Taylor Vortices*, Cambridge Monographs on Mechanics, Cambridge University Press, 1993.

[7] M. Lappa, *Thermal Convection: Patterns, Evolution and Stability*, Wiley, 2009.

[8] T. Ma and S. Wang, *Phase Transition Dynamics in Nonlinear Sciences*, Springer, to appear.

[9] T. Ma and S. Wang, *Dynamic bifurcation and stability in the Rayleigh-Bénard convection*, Commun. Math. Sci., 2(2), 159–183, 2004.

[10] T. Ma and S. Wang, *Rayleigh Bénard convection: Dynamics and structure in the physical space*, Commun. Math. Sci., 5(3), 553–574, 2007.

[11] E. Palm, *Nonlinear thermal convection*, Ann. Rev. Fluid Mech., 7(1), 39–61, 1975.

[12] T. Sengul and S. Wang, *Dynamic transitions of surface tension driven convection*, Physica D., to appear.

[13] T. Sengul and S. Wang, *Pattern formation and dynamic transition for magnetohydrodynamic convection*, submitted.